# Fluorescence of Er$^{3+}$:AlN polycrystalline ceramic

**Larry D. Merkle,[1,*] Anthony C. Sutorik,[2] Tigran Sanamyan,[1] Lindsay K. Hussey,[1,3] Gary Gilde,[2] Christopher Cooper,[2] and Mark Dubinskii[1]**

[1]*U.S. Army Research Laboratory, RDRL SEE M, 2800 Powder Mill Rd., Adelphi, MD 20783, USA*
[2]*U.S. Army Research Laboratory, RDRL WMM E, Building 4600, Aberdeen Proving Ground, MD 21005, USA*
[3]*North Carolina State University, Department of Materials Science and Engineering, Raleigh, NC 27695, USA*
*\*larry.d.merkle.civ@mail.mil*

**Abstract:** We report what we believe to be the first preparation and optical spectroscopy of Er$^{3+}$ doped into bulk AlN ceramic. The material was prepared via hot press sintering of AlN with Er$_2$O$_3$ and [NH$_4$][ErF$_4$], which yielded fully dense, translucent, hexagonal AlN. The Er$^{3+}$ concentration is a small fraction of a percent, and resides in multiple sites, with one type of center dominant. A number of the energy levels of Er$^{3+}$ are identified for this center. The temperature dependent fluorescence lifetime is probably radiative, and on that basis the stimulated emission and absorption cross section spectra are inferred for the $^4I_{13/2} \leftrightarrow {}^4I_{15/2}$ transitions.

©2011 Optical Society of America

**OCIS codes:** (140.3380) Laser materials; (160.5690) Rare-earth-doped materials; (300.2140) Emission.

## References and links

1. A. J. Steckl and J. M. Zavada, "Photonic Applications of Rare-Earth-Doped Materials," MRS Bull. **24**, 33–38 (1999).
2. N. Hirosaki, R.-J. Xie, K. Inoue, T. Sekiguchi, B. Dierre, and K. Tamura, "Blue-emitting AlN:Eu$^{2+}$ Nitride Phosphor for Field Emission Displays," Appl. Phys. Lett. **91**(6), 061101 (2007).
3. G. A. Slack, L. J. Schowalter, D. Morelli, and J. A. Freitas, Jr., "Some Effects of Oxygen Impurities on AlN and GaN," J. Cryst. Growth **246**(3-4), 287–298 (2002).
4. W. J. Tropf, M. E. Thomas, and T. J. Harris, "Properties of Crystals and Glasses," in *Handbook of Optics* 2, (McGraw-Hill, New York, 1995), 33.33–33.34.
5. T. Mah and T. A. Parthasarathy, "Fracture toughness of single crystal YAG," Scr. Metall. Mater. **28**(11), 1383–1385 (1993).
6. E. D. Readinger, G. D. Metcalfe, H. Shen, and M. Wraback, "GaN doped with neodymium by plasma-assisted molecular beam epitaxy," Appl. Phys. Lett. **92**(6), 061108 (2008).
7. G. D. Metcalfe, E. D. Readinger, R. Enck, H. Shen, M. Wraback, N. T. Woodward, J. Poplawsky, and V. Dierolf, "Near-infrared photoluminescence properties of neodymium in *in situ* doped AlN grown using plasma-assisted molecular beam epitaxy," Opt. Mater. Express **1**(1), 78–84 (2011).
8. M. Maqbool, H. R. Richardson, and M. E. Kordesch, "Luminescence from Praseodymium doped AlN thin films Deposited by RF Magnetron Sputtering and the effect of material Structure and Thermal Annealing on Luminescence," J. Mater. Sci. **42**(14), 5657–5660 (2007).
9. R. Weingartner, O. Erlenbach, A. Winnacker, A. Welte, I. Brauer, H. Mendel, H. P. Strunk, C. T. M. Ribeiro, and A. R. Zanatta, "Thermal Activation, Cathode- and Photoluminescence Measurements of Rare Earth doped (Tm, Tb, Dy, Eu, Sm, Yb,) amorphous/ nanocrystalline AlN Thin Films Prepared by Reactive RF-Sputtering," Opt. Mater. **28**(6-7), 790–793 (2006).
10. H. J. Lozykowski, W. M. Jadwisienczak, A. Bensaoula, and O. Monteiro, "Luminescence and Excitation Mechanisms of Pr, Eu, Tb, and Tm ions implanted into AlN," Microelectron. J. **36**(3-6), 453–455 (2005).
11. K. Lorenz, E. Alves, T. Monteiro, M. J. Soares, M. Peres, and P. J. M. Smulders, "Optical Doping of AlN by Rare Earth Implantation," Nucl. Instrum. Methods Phys. Res. B **242**(1-2), 307–310 (2006).
12. D. A. Neumayer and J. G. Ekerdt, "Growth of Group III Nitrides. A Review of Precursors and Techniques," Chem. Mater. **8**(1), 9–25 (1996).
13. L. M. Sheppard, "Aluminum Nitride: A Versatile but Challenging Material," Am. Ceram. Soc. Bull. **69**(11), 1801–1812 (1990).
14. B. Dierre, X. L. Yuan, K. Inoue, N. Hirosaki, R.-J. Xie, and T. Sekiguchi, "Role of Si in the Luminescence of AlN:Eu,Si Phosphors," J. Am. Ceram. Soc. **92**(6), 1272–1275 (2009).
15. B. Han, K. C. Mishra, M. Raukas, K. Klinedinst, J. Tao, and J. B. Talbot, "Investigation of Luminescence from Dy3+ in AlN," J. Electrochem. Soc. **154**(1), J44–J52 (2007).

# Report Documentation Page

| 1. REPORT DATE **07 DEC 2011** | 2. REPORT TYPE | 3. DATES COVERED **00-00-2011 to 00-00-2011** |
|---|---|---|

| 4. TITLE AND SUBTITLE **Fluorescence Of Er3+:AlN Polycrystalline Ceramic** | 5a. CONTRACT NUMBER |
|---|---|
| | 5b. GRANT NUMBER |
| | 5c. PROGRAM ELEMENT NUMBER |

| 6. AUTHOR(S) | 5d. PROJECT NUMBER |
|---|---|
| | 5e. TASK NUMBER |
| | 5f. WORK UNIT NUMBER |

| 7. PERFORMING ORGANIZATION NAME(S) AND ADDRESS(ES) **U.S. Army Research Laboratory, RDRL SEE M,2800 Powder Mill Rd,Adelphi,MD,20783** | 8. PERFORMING ORGANIZATION REPORT NUMBER |
|---|---|

| 9. SPONSORING/MONITORING AGENCY NAME(S) AND ADDRESS(ES) | 10. SPONSOR/MONITOR'S ACRONYM(S) |
|---|---|
| | 11. SPONSOR/MONITOR'S REPORT NUMBER(S) |

**12. DISTRIBUTION/AVAILABILITY STATEMENT**
**Approved for public release; distribution unlimited**

**13. SUPPLEMENTARY NOTES**
**Optical Materials Express, Vol. 2, Issue 1, pp. 1664-1677 (2012)**

**14. ABSTRACT**

**15. SUBJECT TERMS**

| 16. SECURITY CLASSIFICATION OF: | | | 17. LIMITATION OF ABSTRACT | 18. NUMBER OF PAGES | 19a. NAME OF RESPONSIBLE PERSON |
|---|---|---|---|---|---|
| a. REPORT **unclassified** | b. ABSTRACT **unclassified** | c. THIS PAGE **unclassified** | **Same as Report (SAR)** | **15** | |

16. A. M. Hundere and M.-A. Einarsrud, "Effects of Reduction of the Al-Y-O Containing Secondary Phases During Sintering of AlN with $YF_3$ Additions," J. Eur. Ceram. Soc. **16**(8), 899–906 (1996).
17. R. Terao, J. Tatami, T. Meguro, and K. Komeya, "Fracture Behavior of AlN Ceramics with Rare Earth Oxides," J. Eur. Ceram. Soc. **22**(7), 1051–1059 (2002).
18. N. S. VanDamme, S. M. Richard, and S. R. Winzer, "Liquid-Phase Sintering of Aluminum Nitride by Europium Oxide Additives," J. Am. Ceram. Soc. **72**(8), 1409–1414 (1989).
19. N. Kuramoto and H. Taniguchi, "Transparent AlN Ceramics," J. Mater. Sci. Lett. **3**(6), 471–474 (1984).
20. Y. Xiong, Z. Fu, Y. Wang, and F. Quan, "Fabrication of Transparent AlN Ceramic," J. Mater. Sci. **41**(8), 2537–2539 (2006).
21. T. Honma, Y. Kuroki, T. Okamoto, M. Takata, Y. Kanechika, M. Azuma, and H. Taniguchi, "Transmittance and Cathodoluminescence of AlN Ceramics Sintered with $Ca_3Al_2O_6$ as Sintering Additive," Ceram. Int. **34**(4), 943–946 (2008).
22. M. Hirano, K. Kato, T. Isobe, and T. Hirano, "Sintering and Characterization of Fully Dense Aluminum Nitride Ceramics," J. Mater. Sci. **28**(17), 4725–4730 (1993).
23. A. A. Kaplyanskiĭ, A. B. Kulinkin, A. B. Kutsenko, S. P. Feofilov, R. I. Zakharchenya, and T. N. Vasilevskaya, "Optical spectra of triply-charged rare-earth ions in polycrystalline corundum," Phys. Solid State **40**(8), 1310–1316 (1998).
24. A. Lupei, V. Lupei, C. Gheorghe, and A. Ikesue, "Excited states dynamics of $Er^{3+}$ in $Sc_2O_3$ ceramic," J. Lumin. **128**(5-6), 918–920 (2008).
25. L. D. Merkle, N. Ter-Gabrielyan, and V. Fromzel, "Cryogenic Laser Properties of Er:YAG and Er:$Sc_2O_3$ – A Comparison," in *Advanced Solid-State Photonics Meeting*, Technical Digest (CD) (Optical Society of America, 2011), paper AWA2. http://www.opticsinfobase.org/abstract.cfm?URI=ASSP-2011-AWA02.
26. D. M. Gill, J. C. Wright, and L. McCaughan, "Site characterization of rare-earth-doped LiNbO3 using total site selective spectroscopy," Appl. Phys. Lett. **64**(19), 2483–2485 (1994).
27. V. Dierolf, C. Sandmann, J. Zavada, P. Chow, and B. Hertog, "Site-selective spectroscopy of Er in GaN," J. Appl. Phys. **95**(10), 5464–5470 (2004).
28. V. Glukhanyuk, H. Przybylinska, A. Kozanecki, and W. Jantsch, "Site symmetry of erbium centers in GaN," Phys. Status Solidi A **201**(2), 195–198 (2004).
29. S. Yang, S. M. Evans, L. E. Halliburton, G. A. Slack, S. B. Schujman, K. E. Morgan, R. T. Bondokov, and S. G. Mueller, "Electron paramagnetic resonance of $Er^{3+}$ ions in aluminum nitride," J. Appl. Phys. **105**(2), 023714 (2009).
30. B. Edlén, "The Refractive Index of Air," Metrologia **2**(2), 71–80 (1966).
31. V. Yu. Davydov, Yu. E. Kitaev, I. N. Goncharuk, A. N. Smirnov, J. Graul, O. Semchinova, D. Uffmann, M. B. Smirnov, A. P. Mirgorodsky, and R. A. Evarestov, "Phonon dispersion and Raman scattering in hexagonal GaN and AlN," Phys. Rev. B **58**(19), 12899–12907 (1998).
32. M. J. Weber, "Multiphonon Relaxation of Rare-Earth Ions in Yttrium Orthoaluminate," Phys. Rev. B **8**(1), 54–64 (1973).
33. C. R. Powell, *Physics of Solid-State Laser Materials* (AIP Press, 1998), Chap. 9.
34. B. F. Aull and H. P. Jenssen, "Vibronic Interactions in Nd:YAG Resulting in Nonreciprocity of Absorption and Stimulated Emission Cross Sections," IEEE J. Quantum Electron. **18**(5), 925–930 (1982).
35. S. A. Payne, L. L. Chase, L. K. Smith, W. L. Kway, and W. F. Krupke, "Infrared Cross-Section Measurements for Crystals Doped with $Er^{3+}$, $Tm^{3+}$, and $Ho^{3+}$," IEEE J. Quantum Electron. **28**(11), 2619–2630 (1992).
36. M. Thaik, U. Hommerich, R. N. Schwartz, R. G. Wilson, and J. M. Zavada, "Photoluminescence spectroscopy of erbium implanted gallium nitride," Appl. Phys. Lett. **71**(18), 2641–2643 (1997).
37. S. Kim, S. J. Rhee, X. Li, J. J. Coleman, S. G. Bishop, and P. B. Klein, "Excitation Mechanisms of Multiple $Er^{3+}$ Sites in Er-Implanted GaN," J. Electron. Mater. **27**(4), 246–254 (1998).
38. U. Vetter, J. Gruber, A. Nijjar, B. Zandi, G. Öhl, U. Wahl, B. De Vries, H. Hofsäss, and M. Dietrich; the ISOLDE Collaboration, "Crystal field analysis of $Pm^{3+}(4f_4)$ and $Sm^{3+}(4f^5)$ and lattice location studies of $^{147}Nd$ and $^{147}Pm$ in w-AlN," Phys. Rev. B **74**(20), 205201 (2006).
39. S. Yang, S. M. Evans, L. E. Halliburton, G. A. Slack, S. B. Schujman, K. E. Morgan, R. T. Bondokov, and S. G. Mueller, "Electron paramagnetic resonance of $Er^{3+}$ ions in aluminum nitride," J. Appl. Phys. **105**(2), 023714 (2009).
40. A. Kozanecki, V. Glukhanyuk, and H. Przybylinska, "Site-selective spectroscopy of erbium in wider band gap semiconductors," Phys. Status Solidi A **205**(1), 38–42 (2008).
41. J. Akiyama, Y. Sato, and T. Taira, "Laser ceramics with rare-earth-doped anisotropic materials," Opt. Lett. **35**(21), 3598–3600 (2010).
42. J. Akiyama, Y. Sato, and T. Taira, "Laser Demonstration of Diode-Pumped $Nd^{3+}$-Doped Fluorapatite Anisotropic Ceramics," Appl. Phys. Express **4**(2), 022703 (2011).
43. J. B. Gruber, A. S. Nijjar, D. K. Sardar, R. M. Yow, C. C. Russell III, T. H. Allik, and B. Zandi, "Spectral analysis and energy-level structure of $Er^{3+}(4f^{11})$ in polycrystalline ceramic garnet $Y_3Al_5O_{12}$," J. Appl. Phys. **97**(6), 063519 (2005).

## 1. Introduction

Rare-earth doped III-nitrides (AlN, GaN, InN, and solid solutions thereof) have been under investigation recently for a number of optoelectronic applications such as light emitting diodes [1] and field emission displays [2]. These materials are also of potential interest for solid-state lasers (SSL's), particularly at high powers, due to their excellent thermal conductivities, which are at room temperature (RT) at least an order of magnitude higher than those of all conventional laser materials (like YAG) [3]. Some of the III-nitrides also have fracture toughness figures significantly higher than that of YAG, which is exceedingly important for ultimate laser power scaling. For example, at RT the fracture toughness of AlN is 3 MPa*m$^{1/2}$ [4], whereas that of YAG is 2 MPa*m$^{1/2}$ [5]. One of the major challenges associated with rare-earth doped nitrides is the difficulty with which these cations can be uniformly incorporated into the host lattice. One can achieve reasonable concentrations of Nd$^{3+}$, for example, by using molecular beam epitaxy, but only in thin films [6,7]. Other thin film methods include co-deposition of nitride and dopant through radio-frequency sputtering of a mixed metal target [8,9] and ion implantation into previously formed nitride films [10,11]. Although sufficient for preparing samples to study fundamental spectroscopic behavior, these methods are size limited to thin film devices, which are not a feasible approach for scaling diode-pumped SSL's to the large volumes required for high powers. Fabrication of highly transparent rare-earth doped bulk III-nitride materials would represent a tremendous improvement in SSL volume-scaling capability by essentially eliminating a thermal management bottleneck associated with the low thermal conductivity of most solid-state gain media. It is thus of great interest to explore new avenues to bulk doping, and to study the spectroscopic properties of trivalent rare earth ions in bulk nitride ceramics to assess aspects of their laser potential, even before greater effort is put into improved doping and increased ceramic transparency. In this paper, we report our study of the formation and fluorescence properties of Er:AlN polycrystalline ceramic. This particular nitride was selected because it has the greatest thermal stability (under conventional pressures) of the various III-N compounds [12] and so its ceramic sintering behavior is much more developed [13].

To prepare high density Er:AlN ceramic, a source of high purity starting powder with consistent particle size and morphology is needed for uniform sintering at high temperature. Rare-earth doped AlN powders can be prepared with high temperature solid state reactions [14] or from reactions using fluoride-based intermediate precursors prepared from low temperature solution chemistry [15]. The former method typically results in powders which have an undesirable degree of particle growth and necking which impedes powder densification, whereas the latter is a laboratory scale method which would require significant scale-up development to produce amounts of powder amenable to ceramic sintering at the desired size (i.e., 100's of grams to start). Additionally, high temperature sintering of these "low-temperature" powders could result in the dopant exsolution from the host lattice as the ceramic particles increase in grain size and crystallinity during solid state diffusion. In other words, the dopant may have been stabilized kinetically in the host lattice during initial synthesis but does not have high thermodynamic stability with regards to the times and temperatures required for ceramic sintering.

Rather than prepare a doped powder for sintering, we have investigated the doping of AlN with Er$^{3+}$ via a reactive sintering method using a mixture of Er$_2$O$_3$ and [NH$_4$][ErF$_4$] as both sintering aid and dopant ion source. Rare earth compounds are often used as sintering aids for AlN [16], and the strengthening effect of some of these additives has been noted [17]. Much less considered is the impact on ceramic optical properties, largely because of the typical opacity of AlN ceramics. In one isolated report, photoluminescence was studied for AlN ceramic doped with 1-9 wt.% Eu$_2$O$_3$ [18]. AlN, however, is interesting in that despite its hexagonal crystal structure, varying levels of translucency for high density AlN have been reported [19–21]. In our current work we find there is sufficient driving force for Er$^{3+}$ to

migrate into the AlN lattice concurrent with the sintering of the host matrix into a translucent, fully dense ceramic, thereby eliminating the need for a separate synthesis of pre-doped Er:AlN starting powder.

## 2. Experimental

Polycrystalline ceramic of $Er^{3+}$:AlN was prepared by uniaxial hot pressing mixtures of starting powders under inert atmosphere. Starting materials were AlN (99.95%, Noah Technologies, San Antonio, TX, USA;), $Er_2O_3$ (99.9%, Cerac, Milwaukee, WI, USA), both used as received from the manufacturer, and ammonium erbium fluoride, average composition $[NH_4][ErF_4]$, prepared in our laboratory via precipitation on mixing of stoichiometric amounts of $NH_4F$ and $Er(NO_3)_3 \cdot 6H_2O$ dissolved in methanol. The precipitation was performed at room temperature. The product was allowed to equilibrate with stirring in the original solvent for one hour, after which it was collected with vacuum filtration, washed with three successive portions of clean methanol, and air dried in a covered glass evaporation dish. $[NH_4][ErF_4]$ was included to act as a partially sacrificial sintering aid in a manner similar to that of $YF_3$ used previously in AlN sintering [16]. The molar ratio of the starting powders was 0.0008 $[NH_4][ErF_4]$: 0.001 $Er_2O_3$: 0.499 AlN. If all available $Er^{3+}$ successfully dopes into AlN, this would result in 0.6 at. % $Er^{3+}$ with respect to Al. The powders were mixed by suspension in a stirring slurry of ethanol (previously dried over molecular sieves). After 1 hour of stirring with a magnetic stir bar, the slurry was transferred to a rotary evaporator, and the ethanol was removed at 60 °C, 170 mbar, and 60 rpm. The constant rotation of the slurry during evaporation provided for a homogeneous powder cake. The dry powders were passed through a 60 mesh stainless steel sieve and stored in a vacuum desiccator. The size distribution of the powders was measured using a Horiba LA-910 Light Scattering Particle Size Distribution Analyzer on dilute suspensions of sample in deionized water, and values for D50 (median size) and D90 (size such that 90% of the distribution is smaller) were $1.53 \pm 0.07$ µm and $3.49 \pm 0.17$ µm, respectively. Ceramics were formed by hot pressing of powders in a 100 Ton hot press using conventional uniaxial graphite dies and resistively heated graphite heating elements. Approximately 20 g of the formulated powder was loaded directly into a graphite die of 2.25 inch internal diameter. The powder charge was layered top and bottom between two sheets of graphoil and solid graphite spacers. Alternatively, smaller 1 inch diameter disks were also formed by pre-pressing ~3 g powder in a uniaxial stainless steel die followed by cold isostatic pressing at 200 MPa. The smaller green disks were hot pressed by embedding in a mass of graphitic flake which is loaded into the 2.25 diameter die in the same configuration as above. The hot press sintering procedure is the same for either method of powder formation. The sample containing die was loaded into the hot press, and the furnace chamber was heated to 1200 °C under vacuum ($<10^{-3}$ torr). Nitrogen was then backfilled into the chamber and a flow of 5 L/min at 20 kPa (3 psi) was established. The furnace was then taken to 2000 °C and held for sintering under a 50 kN (6 ton) load for 24 h.

Powder X-ray diffraction analysis was performed using a computer controlled Rigaku MiniFlex using Cu-Kα radiation (1.54059 Å) operating at 30 kV and 15 mA with a step size of 0.03 °2θ and scan rate of 1 °2θ/min. Samples were loaded directly into low-background Si sample holders. Sintered ceramic samples were ground to a fine powder using a glass mortar and pestle to avoid crystalline contamination.

Emission and excitation spectra were taken using a Horiba iHR320 monochromator with 1.5-micron blazed grating and liquid nitrogen-cooled Judson extended-range InGaAs photodiode for detection. The fluorescence detection bandwidth was typically 1 nm. The principal excitation source was a Spectra Physics Tsunami Ti:sapphire laser operated CW, and tuned point by point with a typical wavelength increment of 0.2 nm. Excitation into part of the $Er^{3+}$ $^4I_{13/2}$ manifold was accomplished using a Santec TSL-210V diode laser tunable over the range 1510-1630 nm. For fluorescence decay measurements, the sample was excited by a SEO Titan-P pulsed Ti:sapphire laser (pulse duration 12 ns and typically 3-4 mJ per pulse

delivered to the sample) and the signal was analyzed using a Tektronix TDS7104 digital oscilloscope. Low temperature measurements were made at approximately 20 K with the sample mounted in a CTI Cryodyne cryogenic refrigerator. In addition, a few experiments were performed at about 80 K in a liquid nitrogen cryostat.

## 3. Results

### 3.1 Ceramic characterization

Sintered Er:AlN samples were dark brown and translucent enough that large type print can be read through the ~1 mm thick ceramic if backlit with a sufficiently bright light source (Fig. 1 inset). The bulk transmittance is actually rather low, as shown in Fig. 1. This level of translucency does indicate a high density, and in fact samples were measured by Archimedes method to have average densities of $3.245 \pm 0.015$ g/cm$^3$, i. e., ~99.5% of the theoretical density of AlN (3.261 g/cm$^3$) [22]. Since both bulk and apparent densities were found to be nearly identical, density variations are likely due to small amounts of trapped porosity. The formation of translucent AlN has been reported by several groups using heating techniques and sintering aids such as hot pressing with $Ca(NO_3)_2 \cdot 4H_2O$ [19], spark plasma sintering with $CaF_2$ [20], and pressureless sintering under $N_2$ with $Ca_3Al_2O_6$ [21].
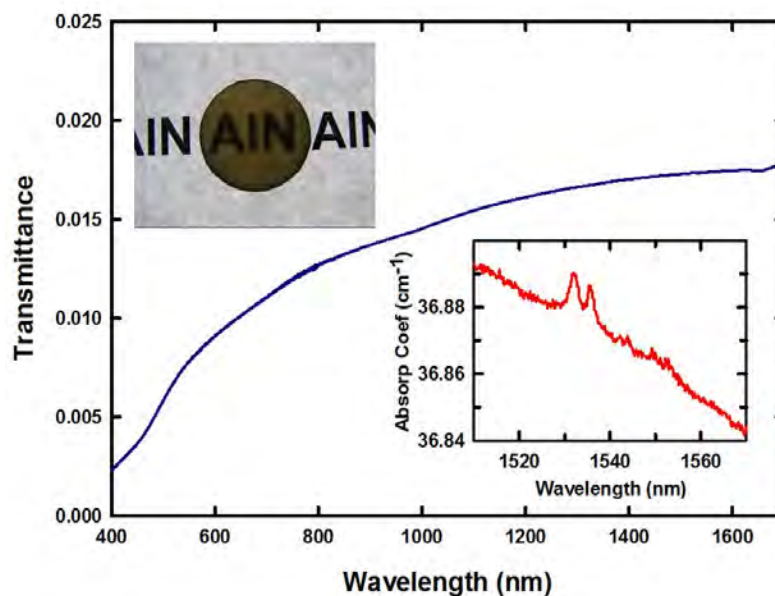


Fig. 1. Transmittance (as a fraction, not percent) of 1.15 mm thick sample of Er:AlN ceramic. Upper left inset: 1 mm thick sample, backlit. Lower right inset: Absorption coefficient in the region of $Er^{3+}$ $^4I_{13/2}$ absorption.

A typical x-ray diffraction pattern of a portion of ground ceramic is shown in Fig. 2. All observed peaks can be assigned to the hexagonal form of AlN (PDF# 25-1133). However, the detection limit of the instrument (~0.1 vol% for highly crystalline samples) is close to the volume that stoichiometric Er-containing compounds could comprise at the current Er-doping level. Thus, powder diffraction by itself is insufficient to confirm that Er:AlN has formed as a single phase, and it is possible that small amounts of residual starting material or unwanted side products could still be present below the detection threshold. In studying the sintering of AlN with 1-10 wt% $Y_2O_3/YF_3$ additives, Hundere and Einarsrud were able to identify several secondary phases depending on sintering conditions and ceramic formulation including $Y_3Al_5O_{12}$, $YAlO_3$, $Y_4Al_2O_9$, $Y_2O_3$ and YN [16]. Investigation of our ceramic grain structure

with electron microscopy revealed an average grain size of 79.6 ± 8.9 µm, but similar to the diffraction experiments, the Er level was so low that the identification of separate phases has proven difficult. To determine if Er-containing secondary phases are occurring in our system, follow-on experiments are needed in which the amount of Er is increased to a level which facilitates both powder diffraction analysis and corroborating electron microscopy and elemental microprobe interrogation of the ceramic gain structure.
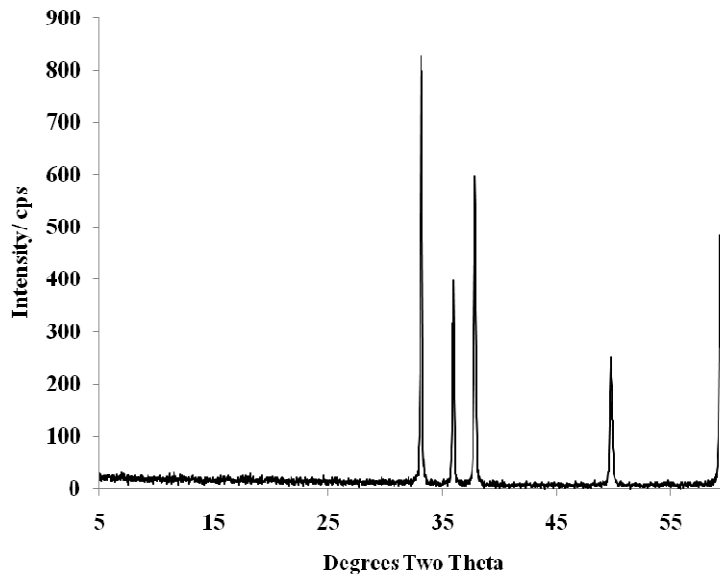


Fig. 2. X-ray diffraction pattern of portion of crushed and ground Er:AlN ceramic.

Samples of formulated powder and sintered ceramic were analyzed by an outside testing company (NSL Analytical, Cleveland, OH, U.S.A.) to determine the levels of Er before and after sintering. The starting powders (measured using Inductively Coupled Plasma/Optical Emission Spectroscopy) possess 0.52 ± 0.02 at. % Er, which is close to that of the intended composition (0.6 at. % Er). In the sintered ceramics, the level of Er was found to be greatly reduced to only 0.0076 ± 0.0034 at. %; these lower levels required analysis using Inductively Coupled Plasma/Mass Spectrometry. This indicates that rather than forming side products, the bulk of Er has likely been lost to high temperature volatilization, likely augmented by the presence of reducing graphite in the sintering furnace. Rare earth evaporation has also been noted in the synthesis of Eu-doped AlN powder heated at 2050 °C [2]. Although this level of $Er^{3+}$ doping is sufficient to study the fluorescence characteristics of the cation in AlN, it is clearly well below the intended composition. Future experiments to increase the amount of Er doping will be focused on reducing the volatility of Er species through reducing the hot pressing temperature to 1800 °C or lower.
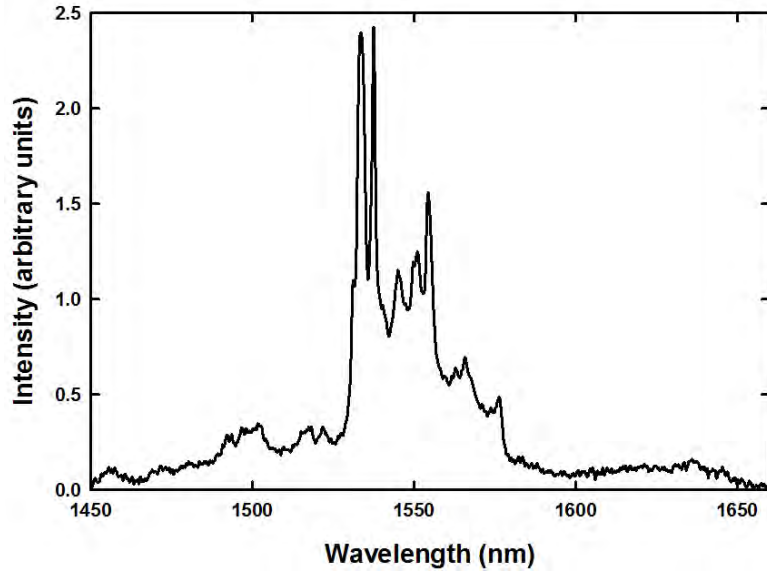
Fig. 3. Typical room temperature fluorescence of Er:AlN upon broadband excitation at 970 nm.
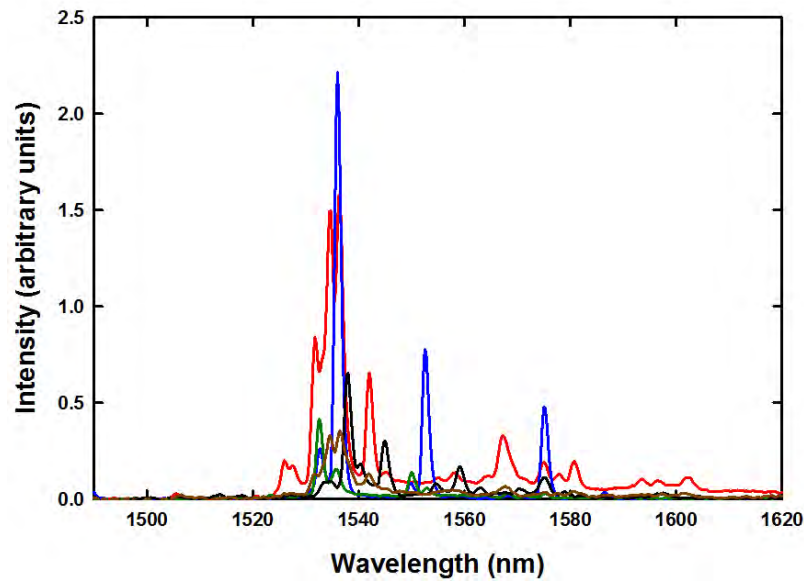


Fig. 4. Er:AlN fluorescence from a single sample at approximately 20 K, for narrow-line excitation into the $^4I_{11/2}$ manifold at several wavelengths: 961.18 nm (green), 962.52 nm (blue), 979.08 nm (brown), 981.02 nm (red), and 986.00 nm (black).

### 3.2 Spectroscopic results

A typical spectrum of the $Er^{3+}$ $^4I_{13/2} \rightarrow$ $^4I_{15/2}$ room temperature fluorescence under 970-nm broadband excitation is shown in Fig. 3. This spectrum changes somewhat with narrow-line excitation and from sample to sample, indicating that Er can reside in more than one environment in ceramic AlN. This is evident upon excitation of a cryogenically cooled sample at several wavelengths near 970 nm using the CW Ti:sapphire laser, as seen in Fig. 4. Experiments in which the $^4I_{13/2}$ fluorescence is integrated over all wavelengths and the

excitation wavelength is scanned over the $^4I_{9/2}$ and $^4I_{11/2}$ manifolds (the two manifolds accessible using a Ti:sapphire laser) indicate that a very few absorption lines give rise to much stronger emission than any others, and emission spectra indicate that most of those lines produce the same spectrum, that shown in red in Fig. 4. This suggests that one kind of Er site is dominant. It has not been possible to check this by absorption spectroscopy, as that absorption is so weak that only two $Er^{3+}$ lines are detectable. Comparing the strengths of those lines (near 1535 nm, Fig. 1 inset) with the estimated absorption cross section spectrum presented in Sec. 3.3, we estimate that the $Er^{3+}$ concentration in the principal spectroscopic sample is ~0.003 at. % with respect to Al, which is reasonably close to the values determined through the elemental analysis discussed above.

Fluorescence and excitation spectra at about 20 K have also been taken on a sample prepared with SiC as a sintering aid in place of $NH_4ErF_4$, with 0.4 at. % Er in the starting material. This sintering aid was less successful, yielding opaque material with only very weak $Er^{3+}$ fluorescence. The signal is, however, sufficient to indicate that the excitation spectra of both samples have the same principal peaks, and upon excitation into one of the strongest excitation lines the fluorescence spectra of the two are essentially identical. Our observed spectra are also very unlike those of $Er:Al_2O_3$ and Er-doped cubic sesquioxides [23–25]. Thus, we conclude that the dominant spectra are due to Er:AlN, not to any residual traces of sintering aid.
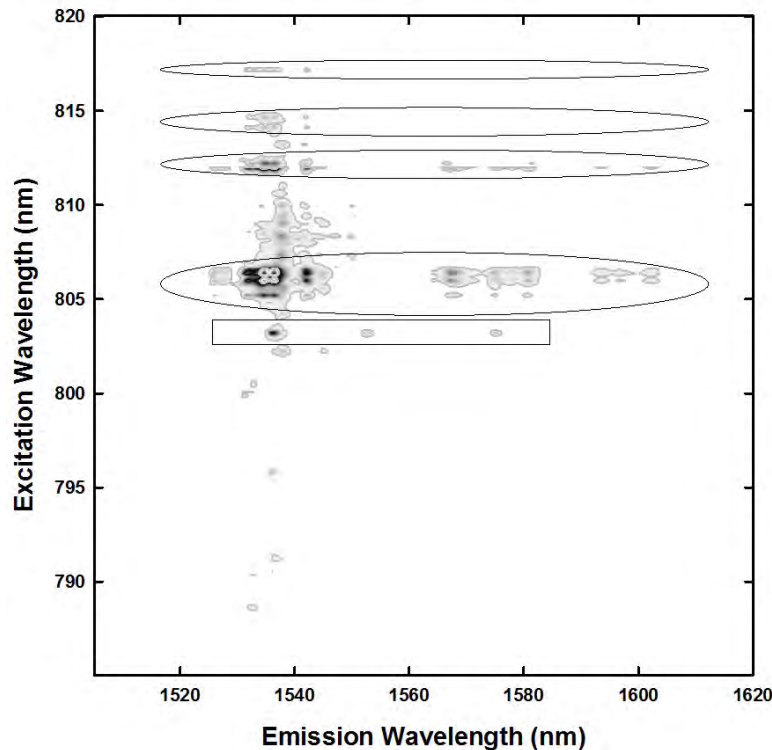


Fig. 5. Spectrofluorometric spectra of Er:AlN at approximately 20 K, for excitation wavelengths covering the $^4I_{9/2}$ manifold. Increasing intensities are denoted by shading that cycles repeatedly through white, gray and black. Ellipses highlight the emission spectra most commonly observed, and thus from the Er site presumed to be dominant. The rectangle highlights the second-most common emission spectrum.

It is possible to get a clearer idea of the multisite spectra by performing spectrofluorometric characterization over the $^4I_{9/2}$ and $^4I_{11/2}$ manifolds. In this technique, the

fluorescence intensity is recorded as a function of both excitation and emission wavelengths [26,27]. The results for a sample temperature of about 20 K are presented in Fig. 5 and Fig. 6. The ellipses highlight excitation wavelengths at which the emission spectrum is that of Er in the site believed to be dominant, that shown in red in Fig. 4. The rectangles in each figure highlight excitation wavelengths giving rise to the second-strongest emission, that shown in blue in Fig. 4. At all other excitation wavelengths the fluorescence is considerably weaker and exhibits no clear or repeated patterns. This suggests that Er exists in many other sites, but not in great numbers.
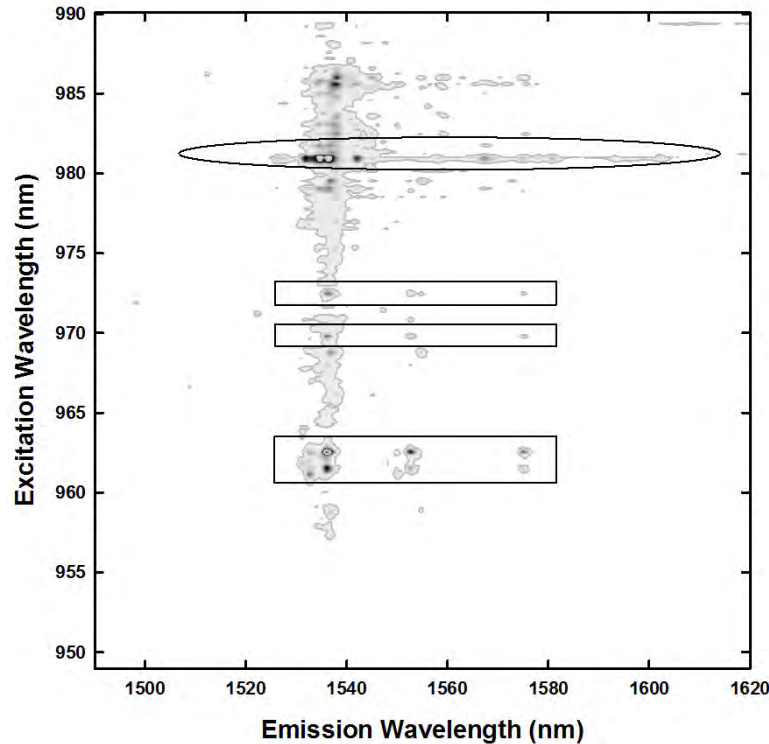


Fig. 6. Spectrofluorometric spectra of Er:AlN at approximately 20 K, for excitation wavelengths covering the $^4I_{11/2}$ manifold. Increasing intensities are denoted by shading that cycles repeatedly through white, gray and black. The ellipse highlights the emission spectra of Er in the presumed dominant site. The rectangles highlight the second-most common emission spectrum.

Each fluorescence spectrum in Fig. 5 has had subtracted from it a smooth band that peaks at 1557 nm and has a full width at half maximum of about 8 nm. It appears in all cryogenic spectra excited over a wavelength range covering at least 780-840 nm, and is inconsistent with $Er^{3+}$ excitation and fluorescence spectra. It is presumably due to a defect in the material, but its investigation is beyond the scope of this paper.

Upon pulsed excitation into the $^4I_{11/2}$ manifold, the $^4I_{13/2}$ emission is only strong enough for quantitative analysis of fluorescence decay for excitation of lines associated with the presumed dominant site. For such excitation, the emission exhibits a single exponential decay for all temperatures between 20 K and room temperature. As shown in Fig. 7, there is a faster initial decay, but tests show that it is due to scattered pump light and that its decay time reflects the detection system's response time. The lifetime decreases smoothly from approximately 5.4 ms to 3.5 ms over that temperature range, as summarized in Fig. 8. The likely interpretation of this trend is discussed below.
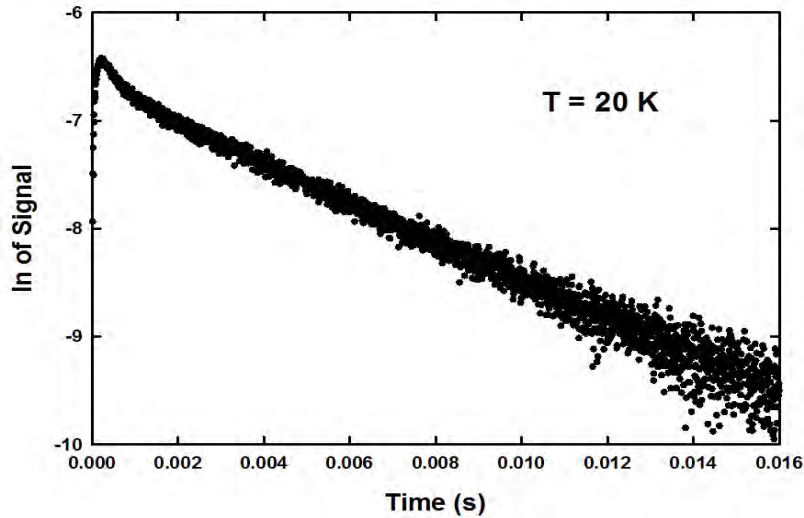
Fig. 7. Fluorescence decay curve of the Er:AlN $^4I_{13/2}$ manifold emission at ~20 K upon pulsed excitation at 805.8 nm.
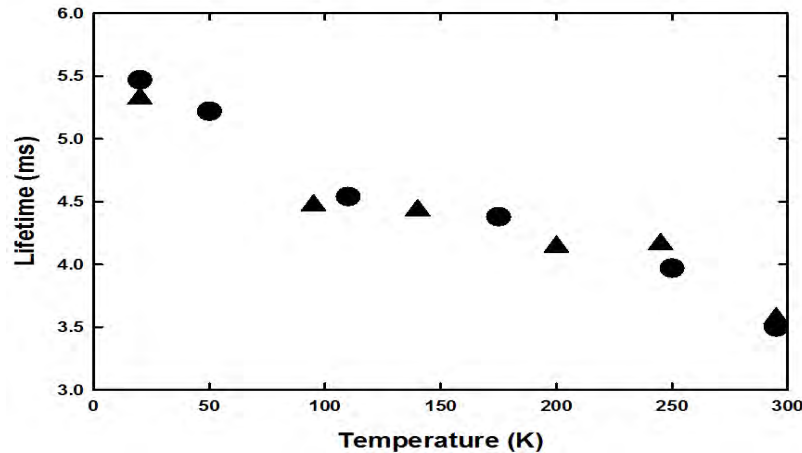


Fig. 8. Fluorescence lifetime of Er:AlN vs temperature, following excitation at 806 ± 0.1 nm (an absorption line of the presumed dominant site). Circles and triangles indicate data for two different emission wavelengths.

### 3.3 Spectroscopic analysis

Only for the site believed to be dominant are there sufficiently consistent spectra to construct a partial energy level scheme. The cryogenic and room temperature $^4I_{13/2} \rightarrow ^4I_{15/2}$ spectra of Fig. 9 can be used to indicate the reasoning used in assigning the levels of those manifolds. The emission peaks at 1602.25 and 1580.75 nm are each at the long-wavelength end of a set of three lines with essentially identical spacing, strongly suggesting that those two lines originate on the lowest level of $^4I_{13/2}$ and end on high-lying levels of $^4I_{15/2}$, and that the lines at ~1599, 1596.75, 1578.00 and 1575.00 nm arise from the second and third lowest levels of $^4I_{13/2}$. It may appear that the peaks at 1593.50 and 1567.25 nm continue this pattern, but in fact their spacings from their respective next-longer lines are not equal. Instead, the pattern of lines just shorter than each of these suggests that they represent transitions from the bottom of $^4I_{13/2}$ to two more states of $^4I_{15/2}$. Although the case is weaker, the positions of lines just shorter

than 1558.25 nm that have grown in by room temperature suggest that the weak line at that wavelength also originates at the bottom of $^4I_{13/2}$ and terminates on another level of $^4I_{15/2}$. The strength of the line at 1542.00 nm at 20 K suggests that it, too, originates at the bottom of $^4I_{13/2}$, thus identifying a probable sixth of the eight levels expected for $^4I_{15/2}$ in the host ions' $C_{3v}$ or lower site symmetry [28,29]. The pair of strong emission lines at 1536.25 and 1534.75 nm at low temperature raises the question as to whether they represent transitions to two closely spaced levels of the ground manifold or from two close levels of the upper. The repetition of doublets with the same spacing at 1527.50 and 1526.00 and (at room temperature) at ~1498 and ~1496.5 nm, and the absence of such spacings for longer-wavelength lines, combine to indicate that it is the lower manifold that has the closely spaced levels. The smooth, rather broad room temperature peak at 1508.7 nm may not appear to fit this pattern, but its detailed shape indicates that it is in fact two closely spaced lines, consistent with the doublets noted above. Spectra at 80 K indicate that its temperature dependence and excitation spectra are consistent with fluorescence from a high-lying level of $^4I_{13/2}$. Using narrower-band pass spectra to refine the peak wavelengths and correcting for the refractive index of air [30], these data indicate the $^4I_{15/2}$ energy levels given in Table 1. These patterns, along with the line at 1531.75 nm and a longer-wavelength shoulder separated from it by a spacing consistent with the above-noted doublets, serve to identify the seven expected $^4I_{13/2}$ levels, as listed in the same table. Low temperature excitation spectra of $^4I_{13/2}$ by the tunable diode laser confirm the emission lines lying within its tuning range, except for showing additional structure around the 1531.75 nm line, which may be due to minority sites. The transitions between the identified levels of these manifolds are indicated in Fig. 9, and show satisfactory agreement with the observed emission spectra.
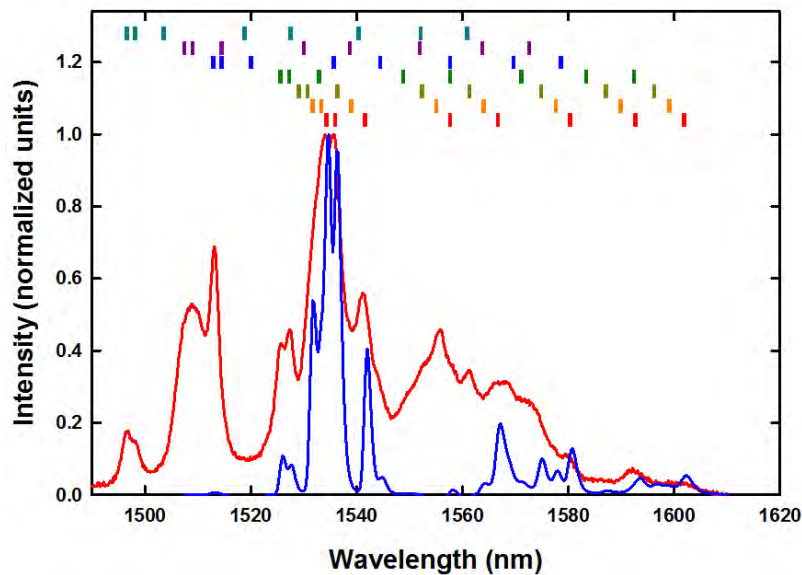


Fig. 9. Normalized room temperature (red trace) and ~20 K (blue trace) fluorescence of the presumed dominant site in Er:AlN. Hash marks denote the wavelengths predicted for transitions between the energy levels in Table 1, with the lowest row of marks (red) indicating transitions from the lowest $^4I_{13/2}$ level to each level of $^4I_{15/2}$, the second row (orange) transitions from the second-lowest $^4I_{13/2}$ level, and so on.

The regions of Fig. 5 highlighted by ellipses indicate that the transitions from the bottom of the $^4I_{15/2}$ manifold to the levels of $^4I_{9/2}$ are most likely 817.14, 814.14, 812.00, 806.00 and 805.20 nm (each to the nearest 0.02 nm). After correction for the refractive index of air, these indicate the $^4I_{9/2}$ levels in Table 1. The data in Fig. 6 show that far fewer excitation

wavelengths associated with the same emission spectrum are discernable for the $^4I_{11/2}$ manifold. In particular, these excitation wavelengths are 989.22, 981.76, 981.02 and 979.08 nm. The lines near 981 nm are separated by the same energy as the two lowest levels of $^4I_{15/2}$, so we have probably detected only three of the six levels expected for $^4I_{11/2}$, with energies given in the same table.

**Table 1. Energy Levels of Er$^{3+}$ in the Presumed Dominant Site in Er:AlN, Inferred from Spectra**

| Manifold | Energy (cm$^{-1}$) | Energy (meV) | Manifold | Energy (cm$^{-1}$) | Energy (meV) |
|---|---|---|---|---|---|
| $^4I_{15/2}$ | 0 | 0 | $^4I_{11/2}$ | 10108 | 1253.3 |
| | 7 | 0.8 | | 10193 | 1263.9 |
| | 31 | 3.8 | | 10213 | 1266.3 |
| | 98 | 12.2 | | — | — |
| | 135 | 16.7 | | — | — |
| | 190 | 23.6 | | — | — |
| | 239 | 29.6 | | | |
| | 275 | 34.1 | $^4I_{9/2}$ | 12,238 | 1517.4 |
| $^4I_{13/2}$ | 6515 | 807.8 | | 12,283 | 1523.0 |
| | 6527 | 809.3 | | 12,315 | 1527.0 |
| | 6538 | 810.7 | | 12,407 | 1538.4 |
| | 6553 | 812.5 | | 12,419 | 1539.9 |
| | 6608 | 819.3 | | | |
| | 6632 | 822.3 | | | |
| | 6680 | 828.3 | | | |

Fluorescence lifetimes that become shorter as the temperature rises, as in Fig. 8, often indicate thermally induced quenching. The familiar process of multiphonon radiationless relaxation is found not to fit the observe temperature dependence at all well, either for the maximum phonon energy (about 940 cm$^{-1}$) or the energies with maximum phonon densities of states (about 660 and 675 cm$^{-1}$) [31]. This is not surprising, as nonradiative decay from the Er$^{3+}$ $^4I_{13/2}$ is usually quite weak. Indeed, to achieve about the right total change in decay rate even without matching the shape of Fig. 8 requires decay rate prefactors at least two orders of magnitude larger than are observed in representative laser materials [32,33]. It is, of course, possible that the lifetime change is due to thermally activated energy transfer to unknown sinks. The observed single-exponential decay at all temperatures makes this possibility appear unlikely, since energy transfer generally only gives exponential decay if it is dominated by diffusion or by transfer between ions that are all separated by the same distance. Neither of these is likely in view of the low Er concentrations observed in this study.

Instead, the strength of the room temperature emission at wavelengths with little or no intensity at 20 K, Fig. 9, suggests that in the present case thermal population of states with particularly strong emission may increase the radiative decay rate enough to explain the lifetime data. The many overlapping emission lines prevent a transition by transition analysis of line strengths, so this possibility has been investigated in an approximate manner, as follows. First the 20-K fluorescence spectrum, corrected for the system's spectral response, was used to calculate the stimulated emission spectrum by the Fuchtbauer-Ladenburg method, using the form of the equation derived by Aull and Jenssen except for removal of the spurious $f_j$ in their Eq. (14) [34]. We made this calculation using the observed 20-K lifetime, on the reasonable assumption that it is at least close to radiative. Next, the room temperature stimulated emission cross section spectrum was calculated by Fuchtbauer-Ladenburg, leaving the radiative lifetime as an adjustable parameter. Next, both cross section spectra were fit to a set of peaks, Gaussian or Lorentzian as needed to fit the data most accurately, to facilitate manipulations needed to compare spectra at the two temperatures. We then broadened each line in the 20-K spectrum to match the width of the corresponding room temperature line, simultaneously dividing each peak height by the same factor so that the line strength is

unchanged. Next, to enable comparison of the lines that originate on the lowest level of $^4I_{13/2}$, we reduced the strength of the 20-K spectrum to reflect the lower thermal population of that level at room temperature. Assuming the line strength of a given transition does not change substantially with temperature, the room temperature spectrum should match the modified 20-K spectrum at lines originating on the lowest $^4I_{13/2}$ level, if those lines are not too strongly overlapped by other transitions. In practice, this means the match should occur for the longest-wavelength transition, at approximately 1602 nm. We compared the spectra and adjusted the room temperature radiative lifetime to achieve a good match at that peak. The resulting lifetime value is about 3.0 ms – much shorter than the 20-K lifetime, and comparable to the observed room temperature lifetime. That is, if the transition of the 1602-nm line is indeed independent of temperature, the total radiative decay rate at room temperature must be considerably higher than at 20 K, indicating that transitions originating on higher levels of the $^4I_{13/2}$ manifold must be, on the whole, much stronger than those originating from the bottom of that manifold.

Clearly, this procedure requires judgment as to whether the longest-wavelength line matches sufficiently well. Nevertheless, this result is sufficient to suggest that the radiative decay rate increases with temperature, and that the observed and radiative lifetimes are similar at room temperature. Combined with the observation that the fluorescence decay curves are single exponentials at all temperatures, this makes it reasonable to assume that the observed lifetimes are indeed radiative, at least to a useful approximation.
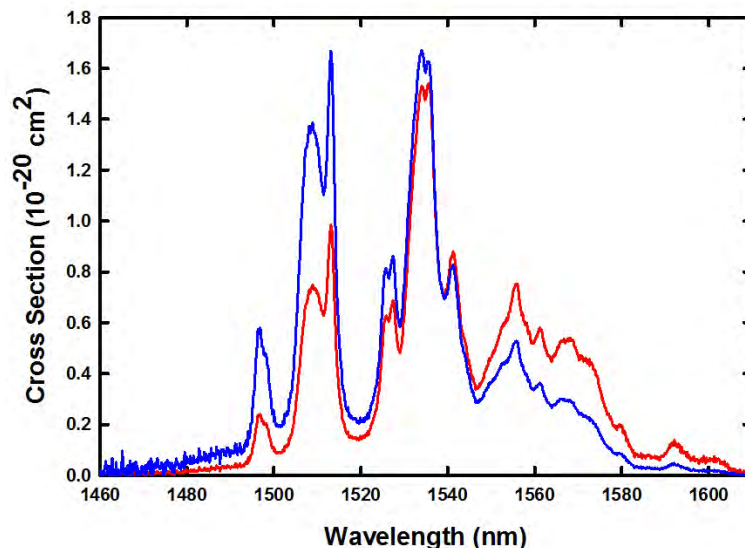


Fig. 10. Room temperature stimulated emission (red trace) and ground state absorption (blue trace) spectra of $Er^{3+}$ in the presumed dominant site of Er:AlN.

The stimulated emission cross section spectrum at room temperature derived on that assumption is presented in Fig. 10. Also shown is the ground state absorption spectrum derived from the stimulated emission by the reciprocity principle [34,35].

## 4. Discussion and conclusions

In this work, we have reported what we believe to be the first preparation and optical spectroscopy of $Er^{3+}$-doped ceramic AlN, including determination of laser-relevant quantities such as cross sections. Considerably more detailed study, beyond the scope of the present work, would be required to identify the nature of the multiple Er sites detected. It is tempting to attribute this multiplicity to the ceramic structure, since there must be many defect sites at

the boundaries between grains, or to traces of other compounds too small to be detected in our x-ray diffraction measurements. However, spectroscopic evidence that rare earth dopants enter more than one type of site in a nitride host is not uncommon, often with one type of site dominant as we believe to be true in the present case [7,27,36–39]. The dominant site for rare earths in AlN is often identified with substitution for Al [38,39], suggesting the possibility that one of the minority spectra is due to Er substituting for N. This multisite occupation is perhaps dependent on the techniques selected for crystal growth and doping, but is certainly not limited to ceramics [40].

Clearly, samples with much lower scattering losses would be required to make the material usable as the gain medium for a SSL. Due to the uniaxial nature of AlN, a grain axis aligning technique implemented during the sintering phase is needed – for example the forced magnetic orientation used by Akiyama and associates to come up with the required "laser transparency" in other anisotropic materials [41,42]. But even at the current state of AlN ceramic development it is of interest to consider whether the spectroscopy of $Er^{3+}$ in AlN is favorable for laser operation. Since one site contributes more prominently to the spectra than any other, our consideration of this question is limited to that site. As Fig. 10 shows, the room temperature absorption cross section around 1535 nm is reasonably strong – comparable to Er:YAG and significantly broader than in that material [35]. This is due in large part to the overlap of closely spaced transitions, but the widths of individual lines (considerably broader than the instrument bandwidth at room temperature) also contribute. Even at low temperature the closely spaced absorption lines match the spectral widths of typical laser diodes usefully well [25]. Thus, resonant diode pumping of $Er^{3+}$ in this AlN site should be quite feasible, assuming samples with significant Er concentration are available. The stimulated emission characteristics are more problematic, as the strongest transitions are rather near the zero line and even the longest wavelength lines are only about half as far from the zero line as in a host like YAG [43]. This is not unexpected, as the crystal field splitting in nitrides is often found to be small compared to that in most oxide hosts [7]. At cryogenic temperatures the longer-wavelength stimulated emission peaks are stronger than at room temperature, and despite the small crystal field splitting the Boltzmann thermal population factors relating absorption to emission cross sections are adequately small. For example, for the emission peak at 1602.4 nm the Boltzmann factor varies from 0.0059 to 0.019 over the temperature range 77 K to 100 K – practical temperatures for cryogenic laser operation. Even for the significantly stronger line at 1580.8 nm the Boltzmann factor is a manageable 0.029 at 77 K. Thus it is possible that this material, with increased Er concentration and employing a technique for forced alignment of the crystalline axes of the grains, can be a useful cryogenic laser material with excellent thermal conductivity to handle high power loading.

## Acknowledgments